Photonics and Nanostructures - Fundamentals and Applications 50 (2022) 101020

Contents lists available at ScienceDirect

Photonics and Nanostructures - Fundamentals and Applications

journal homepage: www.elsevier.com/locate/photonics

Anisotropic absorber and tunable source of MIR radiation based on a black phosphorus-SiC metasurface

Hodjat Hajian [a,*], Ivan D. Rukhlenko [b,c], George W. Hanson [d], Ekmel Ozbay [a,e,f]

[a] NANOTAM-Nanotechnology Research Center, Bilkent University, 06800 Ankara, Turkey
[b] The University of Sydney, Institute of Photonics and Optical Science (IPOS), School of Physics, Camperdown, 2006 NSW, Australia
[c] Information Optical Technologies Centre, ITMO University, Saint Petersburg 197101, Russia
[d] Department of Electrical Engineering, University of Wisconsin, 3200 North Cramer Street, Milwaukee, WI 53211, USA
[e] Department of Electrical and Electronics Engineering, Bilkent University, 06800 Ankara, Turkey
[f] Department of Physics and UNAM-Institute of Materials Science and Nanotechnology, Bilkent University, 06800 Ankara, Turkey

ARTICLE INFO

Keywords:
Black phosphorous
Silicon carbide
Anisotropic
Tunable
Metasurface absorber
MIR radiation source

ABSTRACT

We propose a black phosphorus-silicon carbide (BP-SiC) metasurface with in-plane structural symmetry that can act as both a nearly perfect anisotropic absorber and tunable polarized source of mid-infrared (MIR) radiation. The metasurface is a periodic array of square SiC patches integrated with a BP flake at the top and separated from a bottom reflector by a BaF_2 spacer. We first use analytical calculations and numerical simulations to study the hybridization of the anisotropic plasmons of BP with isotropic phonons of SiC. We also analyze the in-plane characteristics of the resulting hybrid modes of the BP/SiC heterostructure and the BP-SiC metasurface. It is then demonstrated that the proposed metasurface can serve as a nearly perfect anisotropic absorber of MIR radiation with highly selective and omnidirectional features. It is also shown that the metasurface can be used as a polarized MIR source with tunable temperature, which is determined by the thermal equilibrium between the matter and radiation. The suggested design holds promise for artificial coatings that can tune the blackbody thermal signatures, MIR sensing, and highly directional in-plane transportation of the MIR energy.

1. Introduction

Thermal emission by hot objects is an incoherent phenomenon that was explained more than a hundred years ago. According to Planck's law [1], an ideal blackbody incoherently emits a continuous spectrum of electromagnetic radiation, the shape of which is determined solely by the temperature of the blackbody; increasing this temperature intensifies the emission and blueshifts the peak emission wavelength. Kirchhoff's law of heat radiation requires that the spectral directional emissivity $\varepsilon(\lambda, T, \Omega)$ of a body (quantifying the efficiency of its thermal emission as compared to a blackbody) is equal to the spectral directional absorptivity $A(\lambda, T, \Omega)$. It is, therefore, possible to engineer the temporal and spatial coherence of thermal radiation by the thoughtful selection and patterning of the body's material. The realization of this concept about two decades ago led to the experimental demonstration of temporally and spatially coherent thermal emitters [2,3]. Since then, various methods of controlling and manipulating thermal emission based on photonic structures [4], such as photonic crystals [5] and nearly perfect metamaterial/metasurface absorbers (PMAs) [6–8], have been developed. They have found many useful applications, including radiative cooling [9], thermophotovoltaic conversion [10], and thermal camouflaging [11,12]. It has also been demonstrated that incandescent metasurfaces with control over the polarization of their MIR thermal emission can prove useful in spectroscopic applications [13].

In addition to the classification based on the control over the spectrum, polarization, and directivity of the emitted radiation, metastructure-based thermal emitters are also classified according to the material of their building blocks. Several types of plasmonic metastructures, including metal-insulator-metal structures [6,14] and metallic gratings [15], have demonstrated the capacity to control thermal radiation thanks to their support of surface plasmon polaritons (SPPs). Phononic metastructures predominantly composed of polar dielectrics [16], such as SiC [2,3,17–24] and hexagonal boron nitride (hBN) [25–27], are another class of thermal emitters that generate MIR radiation due to the support of hyperbolic phonon polaritons and surface phonon polaritons (SPhPs) in the Reststrahlen band of hBN and SiC.

* Corresponding author.
E-mail addresses: hodjat.hajian@bilkent.edu.tr (H. Hajian), ozbay@bilkent.edu.tr (E. Ozbay).

https://doi.org/10.1016/j.photonics.2022.101020
Received 20 August 2021; Received in revised form 22 January 2022; Accepted 21 March 2022
Available online 28 March 2022

Such metastructures are composed of either unpatterned layers of polar materials [17,18,27] or micrometer-thick resonators on a polar [3, 19–23] or silicon substrate [24]. While thermal emitters based on plasmonic nanostructures are ultrathin due to the nanoscale confinement of the incident light, functional phononic resonators in two-port metasurfaces must be thick enough to enable sufficiently strong light-matter interaction.

The dynamic tunability of plasmonic and phononic thermal emitters further broadens the scope of their practical applications. It is achieved via the integration of the emitters with thermally tunable phase-change materials, such as $Ge_2Sb_2Te_5$ (GST) [18] and vanadium dioxide (VO_2) [28,29], or gate-tunable semiconductors such as InAs [30]. Alternative tunable material is graphene, which can be used in plasmonic metasurfaces as gate-tunable infrared sources [11]. By integrating graphene with phononic metasurfaces based on polar semiconductors, such as SiC [31,32] or hBN [33], one alters their absorptive and emissive properties via the hybridization of the graphene SPPs with phonon polaritons of SiC or hBN. Moreover, one can create a nonvolatile tunable MIR thermal emitter by integrating GST to a silicone carbide (SiC) film or a SiC-based metasurface [18].

The emitters considered so far generate isotropic thermal radiation due to the isotropy of their constituent materials, whereas the generation of polarized radiation demands structures with in-plane asymmetry [3,13,26]. Here, we propose a black phosphorus (BP)-integrated SiC metasurface with in-plane symmetry to achieve nearly perfect anisotropic absorption and thermal emission with tunable characteristics.

BP is a notable member of the two dimensional materials family with outstanding electrical and optical properties. It has a tunable direct bandgap ranging from 1.51 eV for a monolayer BP to 0.59 eV for a five-layer BP, high hole mobility of the order of 10,000 $cm^2\ V^{-1}\ s^{-1}$ (for a monolayer BP), and a thickness-dependent absorption coefficient exhibiting linear dichroism between perpendicular in-plane directions [34,35]. This feature implies that – unlike graphene – BP supports SPPs with dispersions dependent on the direction of propagation [36,37]. These unique properties render BP a great material for infrared optoelectronics [38].

The naturally weak interaction of thin BP films with light can be enhanced by nanopatterning BP flakes grown on a dielectric substrate. This method allows one to fabricate thin BP films with infrared absorption coefficients of up to 35% [39]. The back-coating of the resulting films with an optically thick reflector further yields strong absorption resonances in the infrared range [40–42]. The absorption of BP films is also enhanced by their integration with appropriately designed and aligned metallic [43–46] or dielectric [47–49] gratings via critical coupling. Furthermore, BP metasurfaces can be integrated with functional materials like graphene [50,51] for the enhancement of their absorptive responses. Despite a great deal of research efforts in this field, no study on BP-SiC PMAs and thermal emitters with in-plane structural symmetry and the ability to change polarization and spectral properties has been done so far, to the best of our knowledge.

In this paper, we propose a new type of SiC metasurface composed of square SiC patches covered by a BP flake and separated from an optically thick mirror by a dielectric layer. Through analytical and numerical calculations, we first analyze how the SPP-SPhP hybridization affects the in-plane characteristics of the guided modes supported by a BP/SiC heterostructure and the corresponding BP-SiC metasurface. It is then examined how the hybrid SPP-SPhP modes result in the nearly perfect anisotropic absorption of the metasurface. Finally, it is demonstrated that the BP-SiC PMA can act as a MIR source with tunable thermal features.

2. Theory

Schematic of the proposed BP-SiC PMA is shown in Fig. 1(a). Here AC and ZZ stand for the armchair and zigzag crystallographic directions of BP. The top metasurface is composed of periodically arranged SiC square patches of width $w = 100$ nm, thickness $t = 150$ nm, and lattice constant $p = 130$ nm. The patches are covered with an unpatterned BP flake and separated from an optically thick bottom reflector by a BaF_2 spacer layer with thickness t_s and refractive index $1.3 < n_s < 1.42$ [52]. The room-temperature dielectric constant of SiC is given by the Lorentz model [53].

$$\varepsilon_{SiC} = \varepsilon_\infty \left(1 + \frac{\omega_L^2 - \omega_T^2}{\omega_T^2 - \omega^2 - i\Gamma\omega}\right), \tag{1}$$

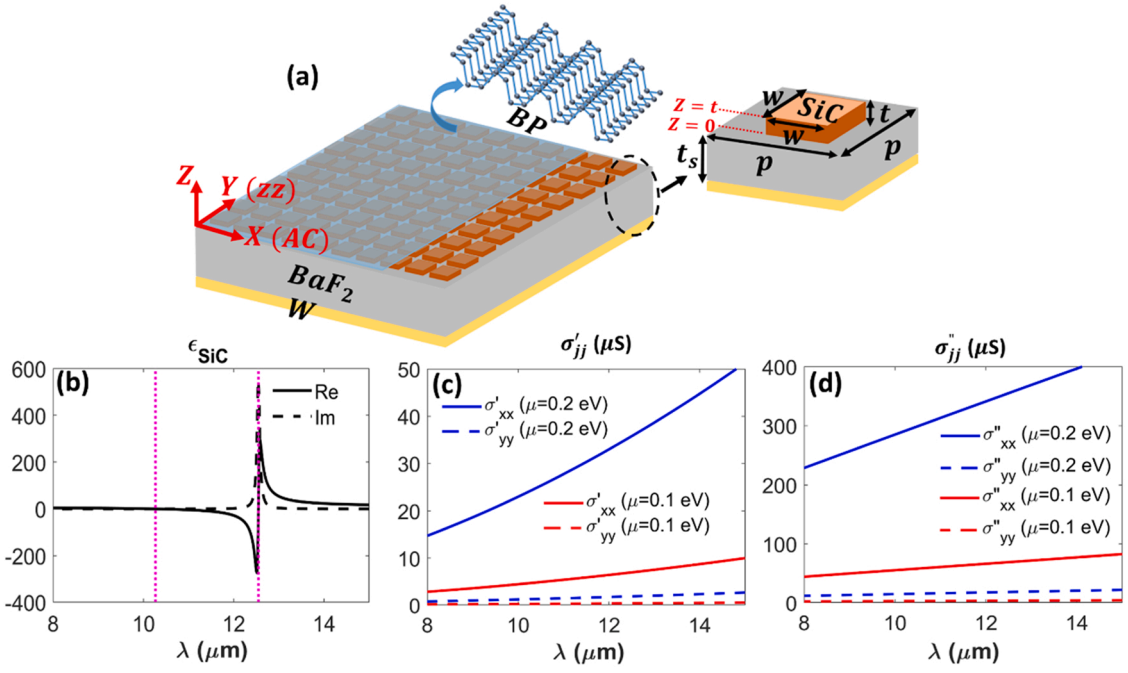

Fig. 1. (a) SiC metasurface covered with a thin BP film and its unit cell without BP (inset), (b) permittivity of SiC with the Reststrahlen band boundaries shown by vertical dotted lines, and (c) real and (d) imaginary parts of optical conductivity of a 3-layer BP for $T = 300$K and different chemical potentials.

where $\omega_L = 974\text{cm}^{-1}$ ($\lambda_L = 10.27\mu\text{m}$), $\omega_T = 797\text{cm}^{-1}$ ($\lambda_T = 12.54\mu\text{m}$), $\Gamma = 4.5\text{cm}^{-1}$, and $\varepsilon_\infty = 6.6$. Fig. 1(b) shows that SiC can support SPhPs within the Reststrahlen band $\lambda_L < \lambda < \lambda_T$, where $\text{Re}(\varepsilon_{\text{SiC}}) < 0$.

When the photon energy is below the bandgap of bulk BP (0.3eV), i.e. $\lambda > 4.132\mu m$, the two components of optical conductivity of *N*-layer BP are given by the Drude model [35–37].

$$\sigma_j(\omega, T) = \frac{iD_j}{\pi(\omega + i\eta/\hbar)}, j = AC\text{or}ZZ, \tag{2}$$

where $D_j = \pi e^2 \sum_{i=1}^{N} n_i/m_i^j$ is the Drude weight, n_i and m_i^j are the electron density and the *j*th effective mass component of the *i*th conduction subband,

$$m_i^{AC} = \frac{\hbar^2/2}{\eta_i^{AC} + \gamma_i^{AC} + \chi_i^2/(2\delta_i)}, \tag{3a}$$

$$m_i^{ZZ} = \frac{\hbar^2/2}{\eta_i^{ZZ} + \gamma_i^{ZZ}}, \tag{3b}$$

where $\eta = 10$ meV, $\eta_i^{AC}(eV.\text{Å}^2) = 0.364\varsigma_i - 1.384$, $\gamma_i^{AC}(eV.\text{Å}^2) = 2.443\varsigma_i + 2.035$, $\chi_i(eV.\text{Å}) = 2.071\varsigma_i + 5.896$, $\delta_i(eV) = 0.712\varsigma_i + 0.919$, $\eta_i^{ZZ}(eV.\text{Å}^2) = 2.699\varsigma_i + 1.265$, $\gamma_i^{ZZ}(eV.\text{Å}^2) = 0.9765\varsigma_i + 2.51$, and $\varsigma_i = \cos[i\pi/(N+1)]$. The electron density of the ith subband is also given by

$$n_i = \left(m_i^{AC} m_i^{ZZ}\right)^{1/2} \frac{k_B T}{\pi\hbar^2} \ln\left[1 + \exp\left(\frac{\mu - E_i}{k_B T}\right)\right], \tag{4}$$

where μ is the chemical potential, $E_i(eV) = 0.58\varsigma_i + 0.505$ is the minimum energy of the *i*-th conduction sub-band, and $n = \sum_{i=1}^{N} n_i$.

The real and imaginary parts of $\sigma_{AC} \equiv \sigma_x$ and $\sigma_{ZZ} \equiv \sigma_y$ of a 3-layer BP flake are plotted in Figs. 1(c) and (d) for $\mu = 0.1\text{eV}$ ($n = 6.4 \times 10^{12}$ cm^{-2}) and $\mu = 0.2\text{eV}$ ($n = 3.28 \times 10^{13}$ cm^{-2}), respectively. Their values are in fair agreement with the recently reported experimental data [54].

Before investigating the absorption characteristics of the BP-SiC PMA, we analytically analyze the dispersion and in-plane modal properties of the hybrid SPP-SPhPs supported by an unpatterned BP/SiC heterostructure. We do this by taking the electric field of the modes in the form of

$$\boldsymbol{E}(x, y, z, t) = e^{i(\beta_x x + \beta_y y - \omega t)} \times$$

$$\begin{Bmatrix} \boldsymbol{E}_- e^{q_s z}, & z < 0 \\ \boldsymbol{E}_+^{\text{SiC}} e^{q_{\text{SiC}} z} + \boldsymbol{E}_-^{\text{SiC}} e^{-q_{\text{SiC}} z}, & 0 < z < t \\ \boldsymbol{E}_+ e^{-q_a(z-t)}, & z > t \end{Bmatrix} \tag{5}$$

where

$$\boldsymbol{E}_\pm = \left(E_{\pm x}, E_{\pm y}, \pm\frac{i}{q_{a,s}}(\beta_x E_{\pm x} + \beta_y E_{\pm y})\right), \tag{6a}$$

$$\boldsymbol{E}_\pm^{\text{SiC}} = E_\pm\left(\beta_y \mp \frac{i\beta_x q_{\text{SiC}}}{\varepsilon_{\text{SiC}}\beta_0}, -\beta_x \mp \frac{i\beta_y q_{\text{SiC}}}{\varepsilon_{\text{SiC}}\beta_0}, \frac{-\beta^2}{\varepsilon_{\text{SiC}}\beta_0}\right), \tag{6b}$$

and where $q_a = \sqrt{\beta^2 - \varepsilon_a\beta_0^2}$, $q_s = \sqrt{\beta^2 - \varepsilon_s\beta_0^2}$, $q_{\text{SiC}} = \sqrt{\beta^2 - \varepsilon_{\text{SiC}}\beta_0^2}$, $\beta^2 = \beta_x^2 + \beta_y^2$, and $\beta_0 = \omega/c$.

By applying the boundary conditions at $z = t$, after some algebra we find the dispersion relation of the guided hybrid modes supported by the air/BP/SiC/sub structure to be of the form

$$\tanh(q_{SiC}t) = -\frac{A}{B}, \tag{7}$$

where coefficients *A* and *B* can be obtained from Ref. [55].

To calculate the temperature of the BP-SiC metasurface from the heat balance equation, we relate its spectral radiance to the spectral directional emissivity as

$$\text{SR}(\lambda, T, \Omega) = \varepsilon(\lambda, T, \Omega)\frac{4\pi\hbar c^2}{\lambda^5}\left[\exp\left(\frac{2\pi\hbar c}{\lambda k_B T}\right) - 1\right]^{-1}, \tag{8}$$

where Ω is the solid angle. By neglecting conduction and convection and assuming the steady state of the metasurface, we can equate the input power P_{in} supplied to it to the total power irradiated by the metasurface. This allows one to find the equilibrium temperature of the metasurface for a fixed input power from the equation

$$P_{in} = \mathscr{A}\iiint \text{SR}(\lambda, T, \Omega)\cos\theta d\Omega \quad d\lambda, \tag{9}$$

where $d\Omega = \sin\theta d\theta d\varphi$ and $\mathscr{A}$ is the surface area of the metasurface.

3. Results and discussion

3.1. Hybrid SPP-SPhP modes of BP/SiC heterostructure

To understand the in-plane features of the resonant modes of the proposed PMA, we first analyze the dispersion and modal characteristics of the hybrid SPP-SPhP modes supported by a BP/SiC heterostructure. The dispersions of the SiC SPhPs, the BP SPPs, and the BP/SiC SPP-SPhPs for $\varepsilon_a = \varepsilon_s = 1$ are plotted in Fig. 2.

Owing to the optical isotropy of SiC, the dispersion of SPhPs supported by a thin SiC film is the same along the *x* and *y* directions [Fig. 2(a)]. On the other hand, the natural anisotropy of BP makes this van der Waals material support highly anisotropic SPPs, the *x* and *y* dispersion branches of which significantly differ [36,37]. This asymmetry is evidenced by Figs. 2(b) and (c), where $\beta_y \gg \beta_x$ for the supported modes. The latter feature makes the excitation of the *y*-propagating modes more challenging than the excitation of the *x*-propagating modes. It is also seen that the wavenumbers of the BP SPPs of a given frequency are reduced with the chemical potential.

Comparison of the red, blue, and black curves in Fig. 2 illustrates that the hybridization of the BP SPPs with the SiC SPhPs creates the anisotropic guided modes of the BP/SiC heterostructure. The blue curves in Fig. 2(b) and 2(c) also show that the hybrid modes can exist within the Reststrahlen band in both *x* and *y* directions for either value of the chemical potential, while for $\lambda < 12.5$ μm and μ = 0.2 eV they are supported only for x direction. Consequently, as we shall see later, the *x*-propagating modes of the BP-SiC PMA with $\mu = 0.2\text{eV}$ create absorption resonances for the transverse magnetic waves below $12.5\mu m$ [Fig. 4(a)]. Moreover, support of the hybrid anisotropic modes is practical for directional guiding purposes [56], as we further elaborate in the following.

Another tool for analyzing the modal features of the hybrid SPP-SPhPs is the FDTD simulation of their in-plane propagation away from the exciting electric dipole. We set a dipole 10 nm on top of the structure's surface and monitor the electric field of the excited modes in the plane that is 5 nm below the source [57]. Fig. 3 shows the results of numerical simulations for five absorption peaks marked with black arrows in Fig. 4.

In agreement with the previous reports [58], Figs. 3(a_1)– 3(a_5) show the propagation of anisotropic SPPs of BP — at small angles relative to the *x*-axis for shorter wavelengths and almost along the *x*-axis for longer wavelengths. The coupling of the BP SPPs with the SiC phonons change the topology of the modes, as evidenced by Figs. 3(b_1)-(b_4) for the three wavelengths within the Reststrahlen band of the BP/SiC structure [54]. Since SiC acts as a low-loss and high-index dielectric at long wavelengths, the modes supported by the unpatterned BP/SiC structure start diverting more and more from the *x*-axis and also weakening with the wavelength [Fig. 3(b_5)].

Once BP is transferred onto the SiC metasurface, the canalization of

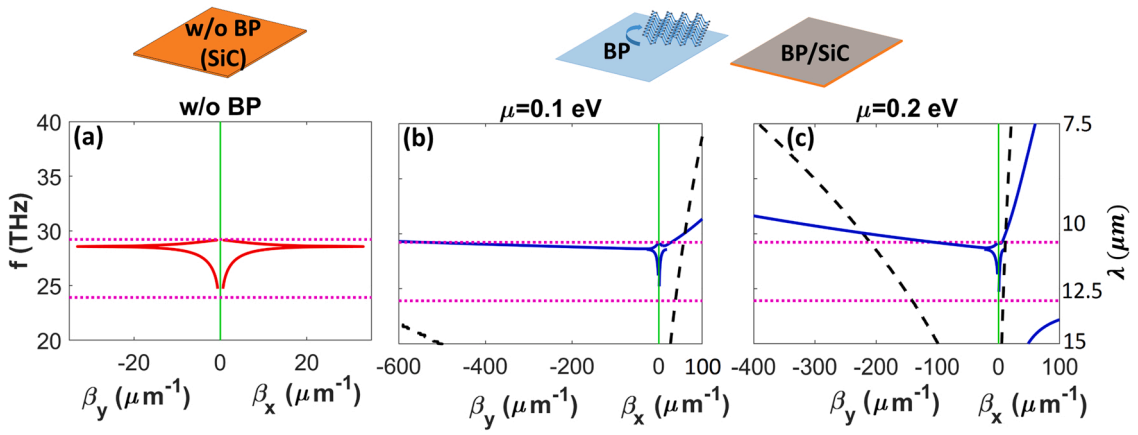

Fig. 2. Dispersions of (a) isotropic SPhPs supported by a 150-nm-thick SiC film and [(b) and (c)] anisotropic SPP-SPhPs supported by BP/SiC heterostructure (solid blue curves) for (b) $\mu = 0.1$eV and (c) $\mu = 0.2$eV. Dashed black curves in (b) and (c) are the dispersions of anisotropic SPPs of a suspended BP flake. Dotted pink lines are the edges of the Reststrahlen band.

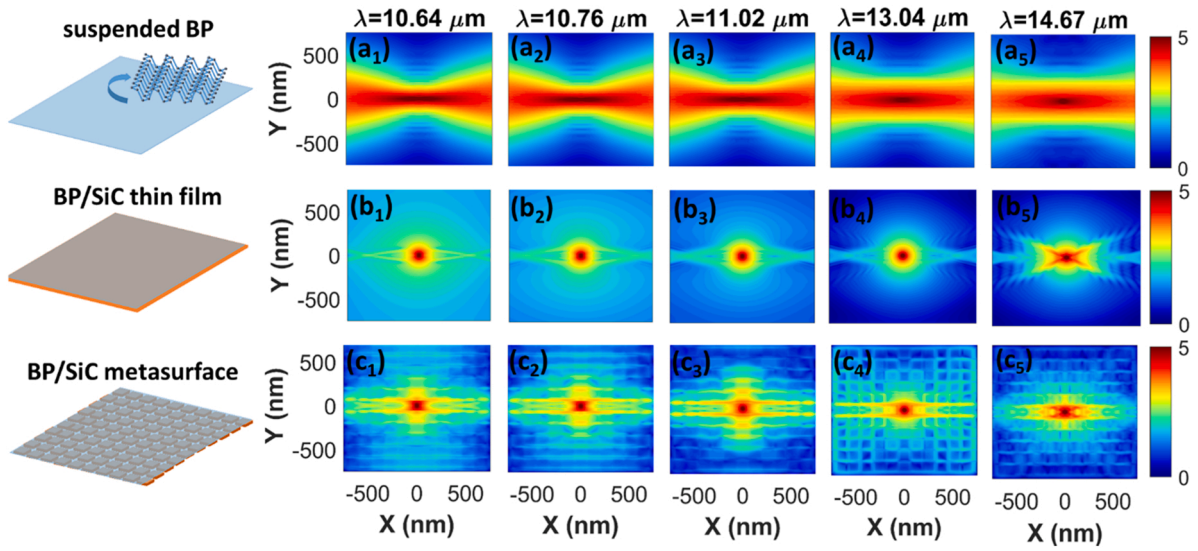

Fig. 3. Density plots of $\log_{10}|\mathbf{E}|$ for electric field $\mathbf{E}$ of dipole-excited (a_1)-(a_5) anisotropic SPPs of suspended BP, hybrid anisotropic SPP-SPhPs of (b_1)-(b_5) BP/SiC heterostructure, and (c_1)-(c_5) BP-SiC metasurface. See text for details.

the hybrid modes is considerably improved [Figs. 3(c_1)-(c_5)]. The modes now propagate predominantly in the x direction while being strongly localized in the y direction. This makes the BP-SiC metasurface very appealing for highly directional guiding and in-plane transportation of the MIR energy.

3.2. *Anisotropic absorption of BP-SiC PMA*

As mentioned earlier, so far only a few groups have demonstrated nearly perfect anisotropic absorption by nanopatterning BP flakes [40–42] and their integration with metallic [43–46] or dielectric gratings [47–49]. One can also increase the functionality of a PMA by coupling an anisotropic BP metasurface to an isotropic graphene sheet and thereby hybridizing the SPPs of the two structures [50,51]. This subsection analyzes the absorption properties of the proposed BP-SiC PMA that emerge due to the hybridization of the SPPs and SPhPs of its two functional materials.

Fig. 4 shows the FDTD-simulated absorption spectra ($A = 1 - R - T$ where $T = 0$) of the BP-SiC metasurface with $t_s = 2\mu$m. The metasurface is illuminated by normally incident transverse magnetic (TM) and transverse electric (TE) waves, which are polarized along the x and y axes, respectively.

Figs. 4(a) and (d) show that the absorption spectra of the TM and TE waves in the absence of the BP flake (dotted brown curves) are the same due to the in-plane symmetry of the SiC metasurface. The addition of the BP flake leads to several notable differences. First, the absorption resonances are strongly modified inside the Reststrahlen band due to the hybridization of the anisotropic SPPs of BP and the isotropic SPhPs of SiC (cf. the solid blue and dashed red spectra with the dotted brown spectrum). Second, these resonances for the TE and TM polarizations are slightly tunable within the Reststrahlen band through modifying the chemical potential [as seen from the insets in Figs. 4(a) and (b)]. However, for $\mu = 0.2$eV an additional resonance (as compared to the response of the bare SiC metasurface) appears inside the Reststrahlen band for each polarization. Besides, for $\mu = 0.1$eV, a nearly perfect TE absorption resonance inside the Reststrahlen band of the metasurface is red-shifted with respect to the w/o BP case. Third, further investigations prove that the absorption spectrum of the BP-SiC metasurface with $\mu = 0$ is almost identical to that of the w/o BP case. Forth, there are strong absorption peaks for the TM waves and $\mu = 0.2$eV outside of the Reststrahlen band [see the solid blue spectra in Fig. 4(a)] while no peaks appear in this region for the lower values of μ [see the dashed red

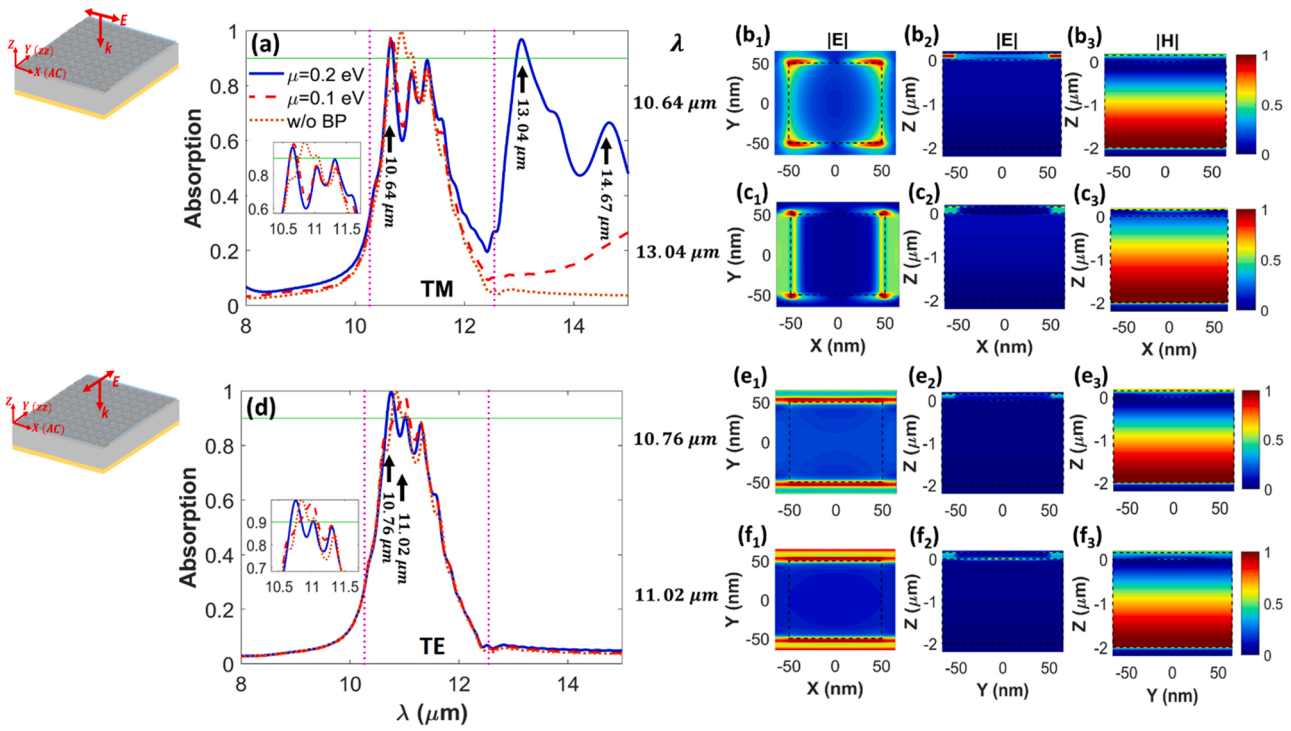

Fig. 4. Absorption spectra of SiC PMA (dotted brown curves) and BP-SiC PMA with $t_s = 2\mu$m, $\mu = 0.2$eV (solid blue curves) and $\mu = 0.1$eV (dashed red curves) excited by normally incident (a) TM and (d) TE waves. Horizontal green lines show $A = 0.9$, vertical dotted lines are the edges of the Reststrahlen band, and the vertical arrows mark the resonance wavelengths of the solid blue spectra discussed in Fig. 3. The density plots (b_{1-3}), (c_{1-3}), (e_{1-3}), and (f_{1-3}) are top and side views of normalized mode profiles at resonance wavelengths. Dashed squares in the top-view profiles show the SiC patch; dashed rectangles in the side-view profiles show the spacer and the SiC film that are located at $-2\mu\text{m} < z < 0$ and $0 < z < 0.15\mu$m, respectively. The electric field of the top-view mode profile is monitored at the plane $z = 0.15\mu$m of the BP flake shown by the dashed-black lines in the side-view profiles.

spectrum in Fig. 4(a)] and the TE waves [see Fig. 4(d)]. Such an active tuning can be achieved by gating [59]. It should also be noted that the pronounced absorption peaks for $\lambda > 12.5\mu$m in Fig. 4(a) come from the excitation of the BP/SiC heterostructure modes traveling in the x direction [Fig. 2(c)]. These results suggest that the proposed BP-SiC metasurface may be a key element of polarized and highly selective MIR absorbers and thermal emitters. Note that in contrast to bulk absorbers with the out-of-plane uniaxial anisotropy [60–62], our metasurface employs an unpatterned anisotropic 2D material integrated with a functional SiC grating. This feature enables gating of the BP flake and makes the metasurface response a hybridization of the plasmonic and phononic responses of BP and SiC due to the increased light-BP interaction. Moreover, it is noteworthy that there are metastructures that can efficiently absorb incident waves, such as a one-dimensional periodic array of metallic cylinders covered with a dielectric medium [63,64] and a single-layer array of bi-anisotropic inclusions [65]. Considering the fabrication simplicity and the ability to absorb MIR radiation > 90% for normal and oblique incidences, the performance of the suggested BP-SiC metasurface can be considered as high as the performances of the metasurfaces reported in Refs. [63–65].

The nature of the absorption resonances can be seen from the electric and magnetic field profiles of the respective excited modes plotted in Figs. 4(b_i), (c_i), (e_i), and (f_i). The profiles correspond to the four wavelengths shown by the arrows in Figs. 4(a) and (d). The anisotropic nature of the resonances is evidenced by the top views of $|\mathbf{E}|$: the TM waves in Figs. 4(b_1) and (c_1) predominantly excite the hybrid modes in the x-direction, whereas the TE waves in Figs. 4(e_1) and (f_1) predominantly excite modes in the y-direction. As further evidenced by the side views of $|\mathbf{E}|$ in Figs. 4(b_2), (c_2), (e_2), and (f_2), the electric field of the modes is mostly localized in the BP-SiC region regardless of the polarization of the excitation wave. Finally, Figs. 4(b_3), (c_3), (e_3), and (f_3) show that the magnetic field is both confined to the spacer layer and strongly enhanced between the adjacent unit cells. This is a clear indication that the excitation of propagating hybrid SPP-SPhPs is the cause of the nearly perfect absorption resonances of the BP-SiC PMA.

The angular response of the proposed BP-SiC PMA is shown in Fig. 5. One can see that the PMA's absorption of TM waves is omnidirectional, as the absorption at the target resonances exceeds almost 80% for relatively large angles of incidence [Figs. 5(a) and (b)]. It is also seen that the width of the target resonance outside of the Reststrahlen band reduces with θ. The PMA's absorption remains omnidirectional for TE waves, and its bandwidth grows with the incidence angle [Figs. 5(c) and (d)]. Note that, similar to other studies [41,42,44,46–49], here we assume that the incident and reflected waves have the same linear polarization. However, owing to the in-plane anisotropy of the BP, there is a possibility of manipulating the polarization of the reflected light using the suggested BP-SiC PMA [66,67]. Furthermore, metasystems composed of BP-SiC and other polar van der Waals materials can also be emplyed for selctive and efficient near-field radiative heat transfers [68].

Fig. 6 shows that, by increasing the spacer thickness from 2 to 3μm, one can selectively decrease the amplitudes of the absorption resonances below 50% for both polarizations inside the Reststrahlen band, while keeping the amplitudes of the TM peaks outside of this band as high as almost 90%. On the other hand, thinning the spacer down to 1 μm reduces the absorption of the PMA for TM polarization to almost 50%. Therefore, 2 μm is the optimal spacer thickness for which the absorption of the metasurface exceeds 90% for both polarizations.

3.3. BP-SiC PMA as a tunable MIR source

As aforementioned, according to Kirchhoff's law, the spectral directional emissivity $\varepsilon(\lambda, T, \Omega)$ of an object must be equal to its spectral directional absorptivity $A(\lambda, \Omega, T)$. Therefore, by considering $A(\lambda, T, \Omega) =$

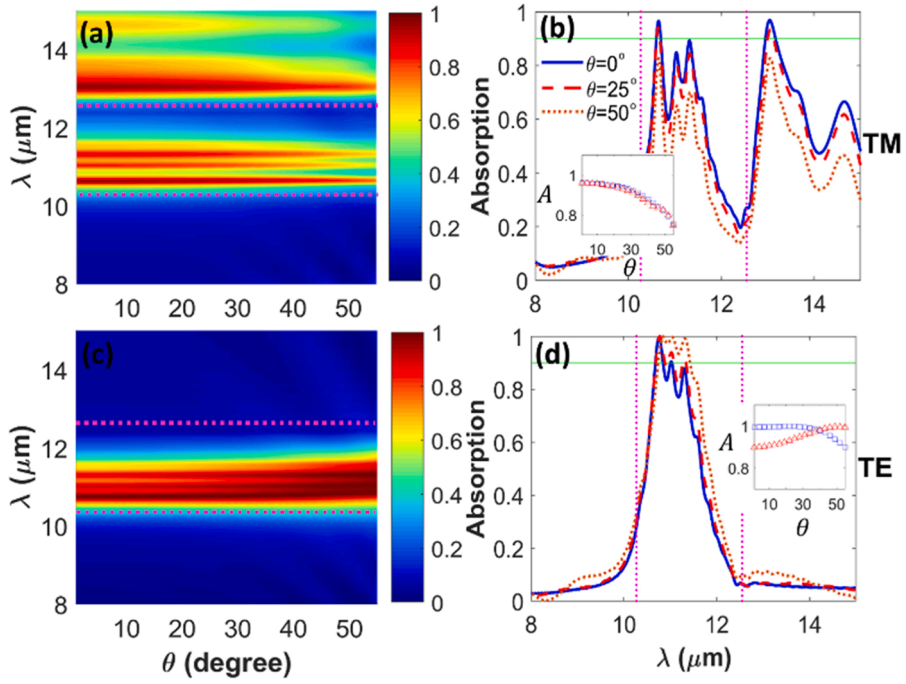

Fig. 5. Absorption spectra of BP-SiC PMA with $t_s = 2\mu$m illuminated by [(a) and (b)] TM and [(c) and (d)] TE waves incident at angle θ. Dotted pink lines are the edges of the Reststrahlen band. Note that blue squares and red triangles in the inset of panel (b) [(d)], respectively, exhibit the dependence of the absorption peak at $10.64\mu m$ [$10.76\mu m$] and $13.04\mu m$ [$11.02\mu m$] on the incident angle.

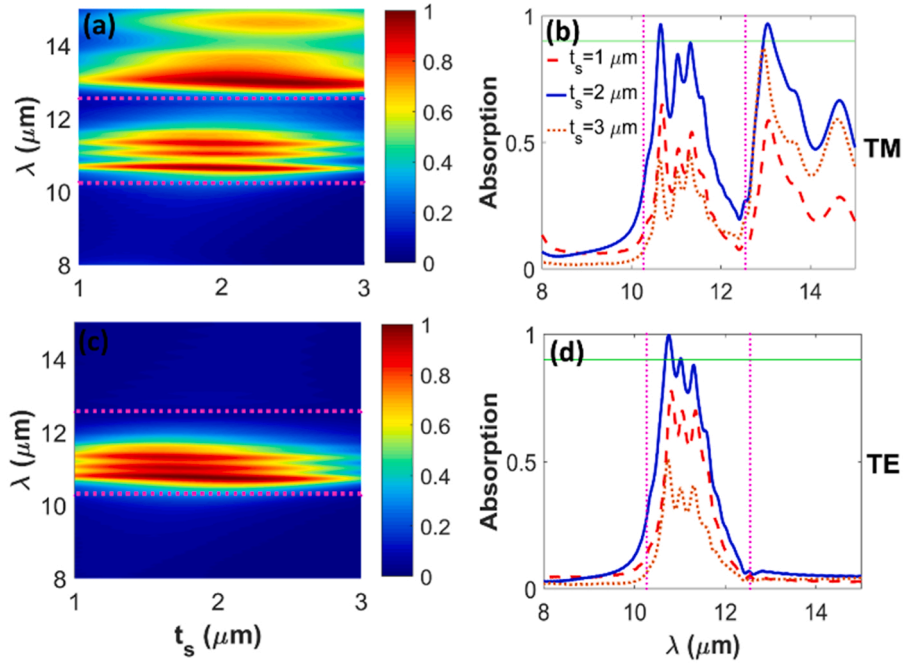

Fig. 6. Absorption spectra of BP-SiC PMA with different spacer thickness t_s illuminated by normally incident [(a) and (b)] TM and [(c) and (d)] TE waves.

$\varepsilon(\lambda, T, \Omega)$ and using Eqs. (8) and (9), which were obtained by neglecting the conduction and convention processes, we can analyze the thermal characteristics of the BP-SiC thermal emitters. The results presented in Fig. 7 are obtained based on numerical simulations for the emission in the normal direction ($\theta = 0$). The device is assumed to be in a vacuum, so that the input power is fully converted to heat and leads to the increase in the device temperature [Fig. 7(a)]. Moreover, considering the optical conductivity of BP at different temperatures in the calculations proves that the absorption/emission spectra of the BP-SiC PMA negligibly depends on the temperature.

The spectral radiance of TM waves at $T = 400$℃ and the equilibrium temperatures of a blackbody, the SiC PMA, and the BP-SiC PMA are shown in Figs. 7(b) and (c), respectively. As expected, at the wavelengths of perfect absorption of the SiC PMA and the BP-SiC PMA, they can also thermally emit infrared radiation as efficient as a blackbody. The comparison of the solid blue, dotted brown and solid black curves in Fig. 7(b) also show that the spectral radiance can be selectively tuned via the chemical potential of BP. Therefore, small input powers (e.g., P_{in} =

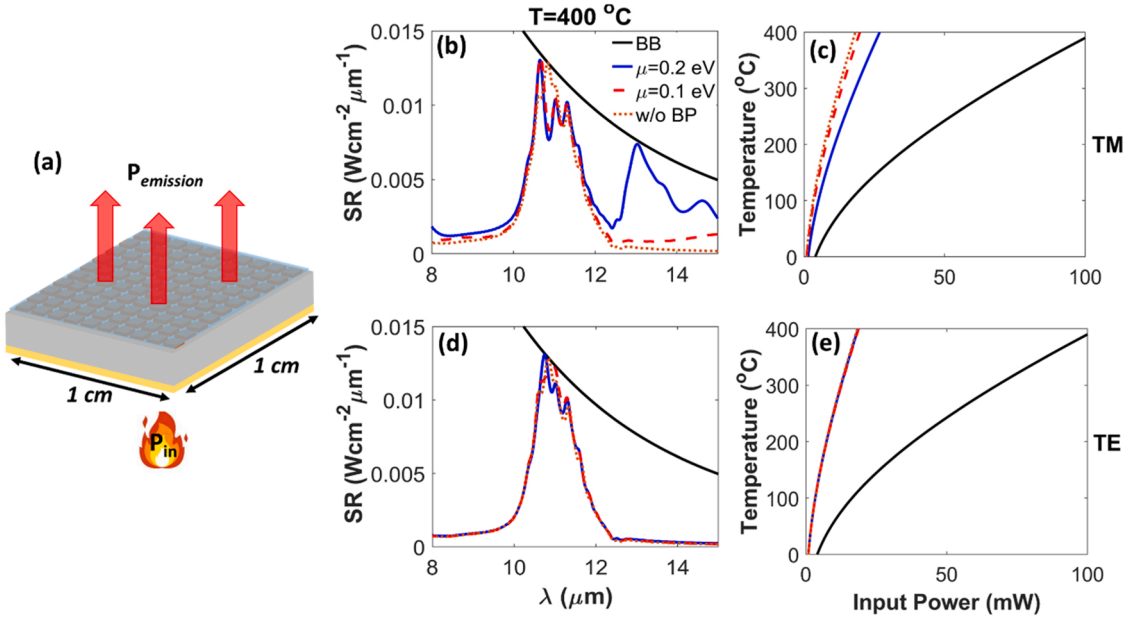

Fig. 7. (a) Schematic of numerical experiment, [(b) and (d)] spectral radiance (SR) of blackbody, BB (solid black curves), SiC PMA (dotted brown curves), and BP-SiC PMA with $\mu = 0.2$eV (solid blue curves) and $\mu = 0.1$eV (dashed red curves) at $T = 400$℃ for TM and TE polarizations at $\theta = 0$, and [(c) and (e)] corresponding equilibrium temperatures versus input power.

17mW) result in much higher equilibrium temperatures of the SiC PMA (397℃) compared to a blackbody (103℃) [cf. the dotted brown and solid black curves in Fig. 7(c)]. The equilibrium temperature of the TM polarized emission can be also conveniently tuned via the chemical potential of BP. For example, $T_{\text{SiC PMA}} = 397$℃ and $T_{\text{BP-SiC PMA},\mu=0.2\text{eV}} = 283$℃ for $P_{in} = 17$mW, as seen from Fig. 7(c).

For TE polarization, the spectral radiance plots and the equilibrium temperatures of the SiC PMA and the BP-SiC PMA are compared with those of a blackbody in Figs. 7(d) and (e). You can see that the PMA can be as effective emitters as a blackbody at the resonance wavelengths. Moreover, for small input powers, PMAs yield much higher equilibrium temperatures than those achievable with a blackbody. However, these temperatures are not tunable for the TE waves. Consequently, the proposed BP-SiC PMA with an in-plane structural symmetry can act as a polarized MIR source with tunable characteristics.

As mentioned above, normal incidence absorption spectrum of the BP-SiC PMA was employed to calculate SR and the equilibrium temperature. By considering the angular response of the structure with $\mu = 0.2$eV, we plot its equilibrium temperature as a function of the input power in Fig. 8(a). As expected, the trends of the curves for TM and TE waves resemble those in Figs. 7(c) and (e). Furthermore, in agreement with the omnidirectionality of the metasurface absorption, the consideration of the angular response is seen to reduce the powers needed to achieve the equilibrium temperature.

Finally, Fig. 8(b) shows that the metasurface absorption can be enhanced at wavelengths outside of the Reststrahlen band, even for small μ, by increasing the number of the BP layers. This becomes evident when the dotted black spectra ($N = 5, \mu = 0.1$eV) and the dashed green spectra ($N = 10, \quad \mu = 0.1$eV) are compared with the solid blue one ($N = 3, \mu = 0.2$eV).

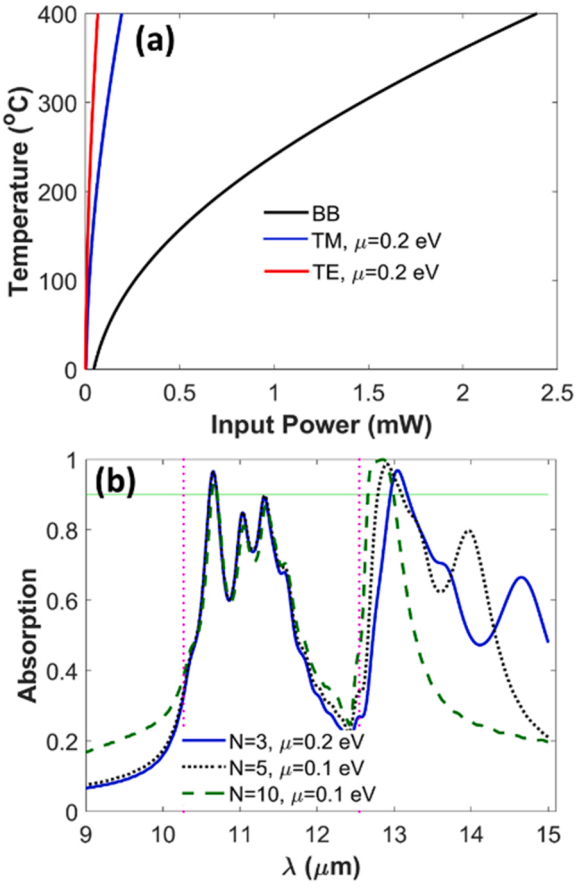

Fig. 8. (a) Equilibrium temperatures of BP-SiC metasurface for $N = 3$, $\mu = 0.2$eV (TM - blue curve, TE - red curve) and blackbody (BB – black curve) versus the input power calculated by considering the angular response of the metasurface. (b) Normal incidence TM absorption spectra of BP-SiC PMA for $N = 3$, $\mu = 0.2$eV (solid blue curve), $N = 5$, $\mu = 0.1$eV (dotted black curve), and $N = 10$, $\mu = 0.1$eV (dashed green curve) with $t_s = 2$ μm.

4. Conclusion

We have designed a new BP-SiC PMA with highly selective, anisotropic, and omnidirectional characteristics. Numerical simulations showed that the PMA is capable of absorbing TM- and TE-polarized MIR waves with efficiency exceeding 80% for oblique incidence up to 55° angle. This efficiently can be improved by increasing the number of the BP layers. According to analytical and numerical calculations, it was also found that the

anisotropic absorption of the PMA owes its existence to the excitation of propagating hybrid SPP-SPhPs of the PMA. The simulated spectral radiance and equilibrium temperature of the PMA further showed that, despite its in-plane symmetry, the BP-SiC PMA can act as a polarized and tunable source of MIR radiation. We believe that the proposed metasurface can find applications in active tuning of thermal radiation, MIR sensing and also highly directional in-plane transportation of the MIR energy.

Declaration of Competing Interest

The authors declare that they have no known competing financial interests or personal relationships that could have appeared to influence the work reported in this paper.

Acknowledgements

E.O. and H.H. acknowledge financial support from TUBITAK project no. 120E422 and partial support from the Turkish Academy of Sciences. I.D.R. thanks the Russian Science Foundation for grant no. 19–13-00332.

References

[1] M. Planck, Ueber das Gesetz der Energieverteilung im Normalspectrum, Ann. Phys. 309 (1901) 553–563.
[2] R. Carminati, J. Greffet, Near-field effects in spatial coherence of thermal sources, Phys. Rev. Lett. 82 (1999) 1660.
[3] J. Greffet, R. Carminati, K. Joulain, J. Philippe Mulet, S. Mainguy, Y. Chen, Coherent emission of light by thermal sources, Nature 416 (2002) 61.
[4] D.G. Baranov, Y. Xiao, I.A. Nechepurenko, A. Krasnok, A. Alù, M.A. Kats, Nanophotonic engineering of far-field thermal emitters, Nat. Mater. 18 (2019) 920.
[5] M.D. Zoysa, T. Asano, K. Mochizuki, A. Oskooi, T. Inoue, S. Noda, Conversion of broadband to narrowband thermal emission through energy recycling, Nat. Photonics 6 (2012) 535.
[6] B.J. Lee, L.P. Wang, Z.M. Zhang, Coherent thermal emission by excitation of magnetic polaritons between periodic strips and a metallic film, Opt. Express 16 (15) (2008) 11328–11336.
[7] Y. Qu, M. Pan, M. Qiu, Directional and spectral control of thermal emission and its application in radiative cooling and infrared light sources, Phys. Rev. Appl. 13 (2020), 064052.
[8] H. Hajian, A. Ghobadi, B. Butun, E. Ozbay, Active metamaterial nearly perfect light absorbers: a review, J. Opt. Soc. Am. B 36 (8) (2019) F131.
[9] L. Zhou, H. Song, J. Liang, M. Singer, M. Zhou, E. Stegenburgs, N. Zhang, C. Xu, T. Ng, Z. Yu, et al., A polydimethylsiloxane coated metal structure for all-day radiative cooling, Nat. Sustain. 2 (2019) 718.
[10] P.N. Dyachenko, S. Molesky, A.Y. Petrov, M. Störmer, T. Krekeler, S. Lang, M. Ritter, Z. Jacob, M. Eich, Controlling thermal emission with refractory epsilon-near-zero metamaterials via topological transitions, Nat. Commun. 7 (2016) 11809.
[11] O. Salihoglu, H.B. Uzlu, O. Yakar, S. Aas, O. Balci, N. Kakenov, S. Balci, S. Olcum, S. Süzer, C. Kocabas, graphene-based adaptive thermal camouflage, Nano Lett. 18 (7) (2018) 4541.
[12] H. Zhu, Q. Li, C. Tao, Y. Hong, Z. Xu, W. Shen, S. Kaur, P. Ghosh, M. Qiu, Multispectral camouflage for infrared, visible, lasers and microwave with radiative cooling, Nat. Commun. 12 (2021) 1805.
[13] L. Wojszvzyk, A. Nguyen, A. Coutrot, C. Zhang, B. Vest, J.-J. Greffet, An incandescent metasurface for quasimonochromatic polarized mid-wave infrared emission modulated beyond 10 MHz, Nat. Commun. 12 (2021) 1492.
[14] X. Liu, Te Tyler, T. Starr, A.F. Starr, N.M. Jokerst, W.J. Padilla, Taming the blackbody with infrared metamaterials as selective thermal emitters, Phys. Rev. Lett. 107 (2011), 045901.
[15] J. Liu, U. Guler, A. Lagutchev, A. Kildishev, O. Malis, A. Boltasseva, V.M. Shalaev, Quasi-coherent thermal emitter based on refractory plasmonic materials, Opt. Mater. Express 5 (2015) 2721.
[16] J.D. Caldwell, L. Lindsay, V. Giannini, I. Vurgaftman, T.L. Reinecke, S.A. Maier, O. J. Glembocki, Low-loss, infrared and terahertz nanophotonics using surface phonon polaritons, Nanophotonics 4 (2015) 44.
[17] B.J. Lee, Z.M. Zhang, Design and fabrication of planar multilayer structures with coherent thermal emission characteristics, J. Appl. Phys. 100 (2006), 063529.
[18] L. Cai, K. Du, Y. Qu, H. Luo, M. Pan, M. Qiu, Q. Li, Nonvolatile tunable silicon-carbide-based midinfrared thermal emitter enabled by phase-changing materials, Opt. Lett. 43 (2018) 1295.
[19] N. Dahan, A. Niv, G. Biener, Y. Gorodetski, V. Kleiner, E. Hasman, Enhanced coherency of thermal emission: beyond the limitation imposed by delocalized surface waves, Phys. Rev. B 76 (2007), 045427.
[20] C. Arnold, F. Marquier, M. Garin, F. Pardo, S. Collin, N. Bardou, J. Pelouard, J. Greffet, Coherent thermal infrared emission by two-dimensional silicon carbide gratings, Phys. Rev. B 86 (2012), 035316.
[21] T. Wang, P. Li, D.N. Chigrin, A.J. Giles, F.J. Bezares, O.J. Glembocki, J.D. Caldwell, T. Taubner, Phonon-polaritonic bowtie nanoantennas: controlling infrared thermal radiation at the nanoscale, ACS Photonics 4 (2017) 1753.
[22] S. Inampudi, J. Cheng, M.M. Salary, H. Mosallaei, Unidirectional thermal radiation from a SiC metasurface, J. Opt. Soc. Am. B 35 (2018) 39.
[23] G. Lu, J.R. Nolen, T.G. Folland, M.J. Tadjer, D.G. Walker, J.D. Caldwell, Narrowband polaritonic thermal emitters driven by waste heat, ACS Omega 5 (2020) 10900.
[24] A. Howes, J.R. Nolen, J.D. Caldwell, J. Valentine, Near-unity and narrowband thermal emissivity in balanced dielectric metasurfaces, Adv. Opt. Mater. 8 (2020), 1901470.
[25] B. Zhao, Z.M. Zhang, Resonance perfect absorption by exciting hyperbolic phonon polaritons in 1D hBN gratings, Opt. Express 25 (7) (2017) 7791–7796.
[26] B. Zhao, Z.M. Zhang, Perfect mid-infrared absorption by hybrid phonon-plasmon polaritons in hBN/metal grating anisotropic structures, Int. J. Heat. Mass Transf. 106 (2017) 1025.
[27] H. Hajian, A. Ghobadi, B. Butun, E. Ozbay, Nearly perfect resonant absorption and coherent thermal emission by hBN-based photonic crystals, Opt. Express 25 (2017) 31970.
[28] M.A. Kats, R. Blanchard, S. Zhang, P. Genevet, C. Ko, S. Ramanathan, F. Capasso, Vanadium dioxide as a natural disordered metamaterial: perfect thermal emission and large broadband negative differential thermal emittance, Phys. Rev. X 3 (2013), 041004.
[29] M.C. Larciprete, M. Centini, S. Paoloni, I. Fratoddi, S.A. Dereshgi, K. Tang, J. Wu, K. Aydin, Adaptive tuning of infrared emission using VO2 thin films, Sci. Rep. 10 (2020) 11544.
[30] J. Park, J. Kang, X. Liu, S.J. Maddox, K. Tang, P.C. McIntyre, S.R. Bank, M. L. Brongersma, Dynamic thermal emission control with InAs-based plasmonic metasurfaces, Sci. Adv. 4 (2018) eaat3163.
[31] K. Li, J.M. Fitzgerald, X. Xiao, J.D. Caldwell, C. Zhang, S.A. Maier, X. Li, V. Giannini, Graphene plasmon cavities made with silicon carbide, ACS Omega 2 (2017) 3640.
[32] P. Rufangura, T.G. Folland, A. Agrawal, J.D. Caldwell, F. Iacopi, Towards low-loss on-chip nanophotonics with coupled graphene and silicon carbide: A review, J. Phys. Mater. 3 (2020), 032005.
[33] H. Hajian, A. Ghobadi, B. Butun, E. Ozbay, Tunable, omnidirectional, and nearly perfect resonant absorptions by a graphene-hBN-based hole array metamaterial, Opt. Express 26 (2018) 16940.
[34] J. Qiao, X. Kong, Z. Hu, F. Yang, W. Ji, High-mobility transport anisotropy and linear dichroism in few-layer black phosphorus, Nat. Commun. 5 (2014) 4475.
[35] T. Low, A.S. Rodin, A. Carvalho, Y. Jiang, H. Wang, F. Xia, A.H. Castro Neto, Tunable optical properties of multilayer black phosphorus thin films, Phys. Rev. B 90 (2014), 075434.
[36] T. Low, R. Roldan, H. Wang, F. Xia, P. Avouris, L. Martin Moreno, F. Guinea, Plasmons and screening in monolayer and multilayer black phosphorus, Phys. Rev. Lett. 113 (2014), 106802.
[37] I. Lee, L. Martin-Moreno, D.A. Mohr, K. Khaliji, T. Low, S. Oh, Anisotropic acoustic plasmons in black phosphorus, ACS Photon 5 (2018) 2208.
[38] Y. Yi, Z. Sun, J. Li, P.K. Chu, X. Yu, Optical and optoelectronic properties of black phosphorus and recent photonic and optoelectronic applications, Small Methods 3 (2019), 1900165.
[39] X. Ni, L. Wang, J. Zhu, X. Chen, W. Lu, Surface plasmons in a nanostructured black phosphorus flake, Opt. Lett. 42 (2017) 2659.
[40] Z. Liu, K. Aydin, Localized surface plasmons in nanostructured monolayer black phosphorus, Nano Lett. 16 (2016) 3457.
[41] F. Xiong, J. Zhang, Z. Zhu, X. Yuan, S. Qin, Strong anisotropic perfect absorption in monolayer black phosphorus and its application as tunable polarizer, J. Opt. 19 (2017), 075002.
[42] S. Xiao, T. Liu, L. Cheng, C. Zhou, X. Jiang, Z. Li, C. Xu, Tunable anisotropic absorption in hyperbolic metamaterials based on black phosphorous/dielectric multilayer structures, J. Light. Technol. 37 (2019) 3290.
[43] Z. Liu, S.A. Wells, S. Butun, E. Palacios, M.C. Hersam, K. Aydin, Extrinsic polarization-controlled optical anisotropy in plasmon-black phosphorus coupled system, Nanotechnology 29 (2018), 285202.
[44] Y.M. Qing, H.F. Ma, T.J. Cui, Strong coupling between magnetic plasmons and surface plasmons in a black phosphorus-spacer-metallic grating hybrid system, Opt. Lett. 43 (2018) 4985.
[45] G. Deng, S. Abedini Dereshgi, X. Song, K. Aydin, Polarization dependent, plasmon-enhanced infrared transmission through gold nanoslits on monolayer black phosphorus, J. Opt. Soc. Am. B 36 (2019) F109.
[46] R. Audhkhasi, M.L. Povinelli, Gold-black phosphorus nanostructured absorbers for efficient light trapping in the mid-infrared, Opt. Express 28 (2020) 19562.
[47] Y.M. Qing, H.F. Ma, T.J. Cui, Tailoring anisotropic perfect absorption in monolayer black phosphorus by critical coupling at terahertz frequencies, Opt. Express 26 (2018) 32442.
[48] T. Liu, X. Jiang, C. Zhou, S. Xiao, Black phosphorus-based anisotropic absorption structure in the mid-infrared, Opt. Express 27 (2019) 27618.
[49] T. Liu, X. Jiang, H. Wang, Y. Liu, C. Zhou, S. Xiao, Tunable anisotropic absorption in monolayer black phosphorus using critical coupling, Appl. Phys. Express 13 (2020), 012010.
[50] J. Nong, W. Wei, W. Wang, G. Lan, Z. Shang, J. Yi, L. Tang, Strong coherent coupling between graphene surface plasmons and anisotropic black phosphorus localized surface plasmons, Opt. Express 26 (2018) 1633.
[51] H. Hajian, I.D. Rukhlenko, G.W. Hanson, E. Ozbay, Hybrid surface plasmon polaritons in graphene coupled anisotropic van der Waals material waveguides, J. Phys. D. 54 (2021), 455102.

[52] H.H. Li, Refractive index of alkaline earth halides and its wavelength and temperature derivatives, J. Phys. Chem. Ref. Data 9 (1980) 161–289.
[53] T.E. Tiwald, J.A. Woollam, S. Zollner, J. Christiansen, R.B. Gregory, T. Wetteroth, S.R. Wilson, A.R. Powell, Carrier concentration and lattice absorption in bulk and epitaxial silicon carbide determined using infrared ellipsometry, Phys. Rev. B 60 (1999) 11464.
[54] S. Biswas, W.S. Whitney, M.Y. Grajower, K. Watanabe, T. Taniguchi, H.A. Bechtel, G.R. Rossman, H.A. Atwater, Tunable intraband optical conductivity and polarization-dependent epsilon-near-zero behavior in black phosphorus, Sci. Adv. 7 (2021) eabd4623.
[55] H. Hajian, I.D. Rukhlenko, G.W. Hanson, T. Low, B. Butun, E. Ozbay, Tunable plasmon-phonon polaritons in anisotropic 2D materials on hexagonal boron nitride, Nanophotonics 9 (2020) 3909.
[56] Deng-Yun Lu, Wei Li, Hu Zhou, Xia Cao, Kai-Jun Wang, Hao-Jie Luo, Jian-Bo Lia, Xin-Min Zhang, Meng-Dong He, Liang Xu, Jian-Qiang Liu, Black phosphorus/waveguide terahertz plasmonic structure for ultrasensitive tunable gas sensing, Photonics Nanostruct. Fundam. Appl. 46 (2021), 100946.
[57] Lumerical Inc (available at: ⟨https://www.lumerical.com/products/⟩).
[58] A. Nemilentsau, T. Low, G. Hanson, Chiral and Hyperbolic Plasmons in Novel 2-D Materials in Carbon-Based Nanoelectromagnetics, Elsevier, 2019, pp. 119–138.
[59] B. Deng, V. Tran, Y. Xie, H. Jiang, C. Li, Q. Guo, X. Wang, H. Tian, S.J. Koester, H. Wang, J.J. Cha, Q. Xia, L. Yang, F. Xia, Efficient electrical control of thin-film black phosphorus bandgap, Nat. Commun. 8 (2017) 14474.
[60] X. Jiang, T. Wang, Q. Zhong, R. Yan, X. Huang, Ultrabroadband light absorption based on photonic topological transitions in hyperbolic metamaterials, Opt. Express 28 (2020) 705–714.
[61] I.S. Nefedov, C.A. Valagiannopoulos, S.M. Hashemi, E.I. Nefedov, Total absorption in asymmetric hyperbolic media, Sci. Rep. 3 (2013) 2662.
[62] X. Wu, C.A. McEleney, M. González-Jiménez, R. Macêdo, Emergent asymmetries and enhancement in the absorption of natural hyperbolic crystals, Optica 6 (2019) 1478–1483.
[63] Y. Ra'di, V.S. Asadchy, S.A. Tretyakov, Total absorption of electromagnetic waves in ultimately thin layers, IEEE Trans. Antennas Propag. 61 (2013) 4606–4614.
[64] C.A. Valagiannopoulos, S.A. Tretyakov, Symmetric absorbers realized as gratings of PEC cylinders covered by ordinary dielectrics, IEEE Trans. Antennas Propag. 62 (2014) 5089–5098.
[65] Z. Tagay, C. Valagiannopoulos, Highly selective transmission and absorption from metasurfaces of periodically corrugated cylindrical particles, Phys. Rev. B 98 (2018), 115306.
[66] W. Xin, H.B. Jiang, T.Q. Sun, X.G. Gao, S.N. Chen, B. Zhao, J.J. Yang, Z.B. Liu, J. G. Tian, C.L. Guo, Optical anisotropy of black phosphorus by total internal reflection, Nano Mater. Sci. 1 (2019) 304–309.
[67] C.A. Valagiannopoulos, M. Mattheakis, S.N. Shirodkar, E. Kaxiras, Manipulating polarized light with a planar slab of black phosphorus, J. Phys. Commun. 1 (2017), 045003.
[68] H. Hajian, I.D. Rukhlenko, V. Erçağlar, G.W. Hanson, E. Ozbay, Epsilon-near-zero enhancement of near-field radiative heat transfer in BP/hBN and BP/a-MoO_3 parallel-plate structures, Applied Physics Letters 120 (2022), 112204.